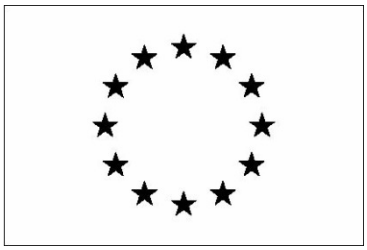

Grant Agreement number: **248095**

Project acronym: **Q-ESSENCE**

Project title: **Quantum Interfaces, Sensors, and Communication based on Entanglement**

Funding Scheme: **Collaborative Project (Large-Scale Integrating Project)**

DELIVERABLE REPORT

Deliverable no.:	**D1.4.4**
Deliverable name:	**Proposal for nonlinear interferometry at the interface of nanomechanics and atomic ensembles**
Workpackage no.	**WP1.4**
Lead beneficiary	**UULM**
Nature	**R = Report**
Dissemination level	**PU = Public**
Delivery date from Annex I (proj month)	**30/04/2013**
Actual / forecast delivery date	**30/04/2013**
Status	**submitted**

D1.4.4

Proposal for nonlinear interferometry at the interface of nanomechanics and atomic ensembles: Report on a theoretical study analysing the capabilities of nonlinear interferometers applied to the measurement of nanomechanics

Currently the field of nano-mechanical systems is rapidly evolving. So far there are several concepts for readout strategies via the interface between quantum states of light and nanomechanics. The interaction of light with atomic ensembles is formally very similar to the light-matter interface, and has already shown within Q-essence how non-linearities enable quantum enhanced read-out even beyond the Heisenberg limit (Deliverable D1.4.1). We therefore used the interaction between light and the quantum state of atomic ensembles in quantum memories as model for the analysis of possible future scenarios for light-nanomechanics coupling.

In particular, we have analysed the problem of estimating the phase associated to a nonlinear evolution which can be obtained by measurement-induced nonlinearities in our atomic-ensemble based quantum memory. In contrast to previous work previous work now different interactions apply. By means of optical interaction with the atomic ensemble, each n photon term in a quantum state of light can be made evolving through a coefficient proportional to $\cos(2J\ n^{1/2})$, with the possibility of producing Schroedinger cat states directly. From a metrological perspective, the interest is in the precision with which the parameter J, associated to the strength of the interaction, can be estimated. We have found that this precision, as quantified by the inverse of the Fisher information, scales worse than the standard quantum limit $(4I)^{-1/2}$, where I is the intensity of the probe state. Along the lines discussed in [1] we have identified the origin of this reduced scaling in the fact that J is associated to a nonlinear term $n^{1/2}$, differently from the case of Deliverable D1.4.1 for which the nonlinear phase χ is associated with n^2. Our results have highlighted that a nonlinear quantum interaction does not generally lead to an improved scaling with respect classical resources.

The interface between atomic and nano-mechanical ensembles was due to lack of time not studied in detail, also due to delays in experiments. Detailed analysis was however performed for the interactions in atomic-ensembles, as they are of significant relevance to the experiment with quantum memories using atomic ensembles. The non-linearities in these systems however turned out to be not useful for quantum metrology.

Publication:

[1] Animesh Datta & Anil Shaji, QUANTUM METROLOGY WITHOUT QUANTUM ENTANGLEMENT, Modern Physics Letters B, Vol. 26, No. 18 (2012) 1230010.

Brief Review

Modern Physics Letters B
Vol. 26, No. 18 (2012) 1230010 (27 pages)

DOI: 10.1142/S0217984912300104

World Scientific
www.worldscientific.com

QUANTUM METROLOGY WITHOUT QUANTUM ENTANGLEMENT

ANIMESH DATTA

Clarendon Laboratory, Department of Physics,
University of Oxford, OX1 3PU, UK
animesh.datta@physics.ox.ac.uk

ANIL SHAJI

School of Physics, IISER TVM, CET Campus,
Thiruvananthapuram, Kerala 695016, India

Received 6 February 2012
Revised 20 May 2012

We scrutinize the role of quantum entanglement in quantum metrology and discuss recent advances in nonlinear quantum metrology that allow improved scalings of the measurement precision with respect to the available resources. Such schemes can surpass the conventional Heisenberg limited scaling of $1/N$ of quantum enhanced metrology. Without investing in the preparation of entangled states, we review how systems with intrinsic nonlinearities such as Bose–Einstein condensates and light-matter interfaces can provide improved scaling in single parameter estimation.

Keywords: Quantum metrology; quantum entanglement; Bose–Einstein condensates; light-matter interfaces.

1. Introduction

Precision measurements of physical parameters is very important for science, technology and commerce. From distinguishing trace chemicals to identifying malignant cells without damaging benign ones in biological samples, measurements of various kinds are some of the most immediate technological challenges of our times. Detection of extremely small quantities such as the amplitude of a passing gravitational wave or the electron dipole moment lie at the forefront of modern physics. Crucial to all these advances is the precision attainable in any measurement.

The estimation of all parameters associated with Hamiltonian dynamics can be cast into a phase estimation. The precision of the estimate is quantified by the variance of the estimator. The standard quantum limit (SQL), also known as the shot noise limit, for the estimation of phase of a quantum-mechanical oscillator is

given by

$$\Delta\phi = \frac{1}{N^{1/2}}, \quad \text{for} \quad N \gg 1\,, \tag{1}$$

where N is the number of excitations in the oscillator. The prototypical precision measurement is of an unknown phase in an interferometer. The SQL is a consequence of a Mandelstamm–Tamm[1] type uncertainty relation that links a parameter like phase or time that has no corresponding quantum mechanical operator with an observable like number of excitations or energy. This is in close analogy with Heisenberg type uncertainty relations between pairs of noncommuting observables. The parameter-based uncertainty relations have a fundamental a role in quantum mechanics, derived from the Heisenberg uncertainty relations. The limiting factor in the precision of estimating parameters turns out to be the inescapable fact that ultimately the device is really quantum mechanical subject to uncertainty relations and quantum back action. As such, the SQL and the allied scaling is the benchmark against which all quantum-enhanced schemes of metrology are judged. The point of this review is to explore the strategies and resources required to go beyond the paradigm of a classical measurement strategy, and from the outset treat the estimation process as quantum mechanical so as to see how one may go beyond the SQL.

The field of quantum metrology concerns itself with the enhanced precision in the parameter estimation that is made possible by quantum mechanics. The original motivation for investigating the limits of the performance of an interferometer was for the detection of gravitational waves, and the notion of quantum nondemolition measurements was developed that circumvent the deleterious effects of quantum back-action.[2–4] Quantum nondemolition measurements, in fact, inquire into some of the deepest questions in quantum mechanics, and have since 1980s proliferated into other areas of quantum mechanics such as quantum measurement theory. The early work of Braginsky, Thorne, Unruh and others led to the proposal by Caves of injecting squeezed light instead of vacuum into the unused input ports of an interferometer to suppress the intrinsic quantum noise associated with any interferometric estimation process.[5] Squeezed states are unmistakably quantum states of light in which the uncertainty of one the quadratures is reduced at the expense of the uncertainty of the other. Their use is motivated by the realization that it is the phase fluctuations in the quantum vacuum that enter the empty port of the interferometer that translate to fluctuations in the amplitude (detector clicks) at the output end. Therefore, sending in squeezed states with reduced uncertainty in the phase quadrature into the empty port translates to reduced uncertainties at the detector. After three decades of persistent advances, the GEO 600 observatory has recently provided one of the first practical applications of squeezed states in quantum technology.[6]

One of the central themes in quantum and classical metrology is the scaling of the measurement uncertainty with the resources invested. Using the fact that most measurement schemes can be mapped to the phase estimation problem, the

resources are typically quantified by N which can stand for number of excitations, quanta, particles etc. depending on the details of the measurement scheme discussed. Squeezed state inputs in one of the arms of an interferometer promise an improved scaling[5,7] of

$$\Delta\phi = \frac{1}{N^{3/4}}, \quad \text{for } N \gg 1\,, \tag{2}$$

in the precision of the estimating the phase by suppressing the noise in one of the quadratures as mentioned above. Better scaling than this is actually possible,[a] and the Heisenberg limit, as this scaling has come to be known, is given by[9]

$$\Delta\phi = \frac{1}{N}\,. \tag{3}$$

It is generally accepted that quantum correlations in the form of quantum entanglement between the N units of a quantum probe is necessary to attain this limit. Canonical examples of states that attain this limit include entangled states such as the two-mode squeezed,[10] Schrödinger cat,[11] and $N00N$ states.[12,13] It has been suggested that this is a true quantum limit, and there is no way that this can be beaten.[14] That however is only true in the restricted case of when the Hamiltonian governing the parameter dependent evolution of the quantum probe is linear and acts independently on each of the N units that make up the probe. The role of nonlinear interactions in providing enhanced scalings to the estimation of parameters will be discussed in detail in this review.

Inseparable from the discussion of nonlinear interactions is the role of entanglement in attaining the enhanced scalings for the measurement precision. Often entanglement is pointed out as the main reason behind why quantum states of the probe can perform better than classical ones in parameter estimation. The actual situation is more involved, since metrological improvement does not change monotonically with respect to the entanglement content of the probe state. There exist states with far more bipartite entanglement than the Schrödinger cat state, upto $N/2$ ebits for equal bipartite splits, that are useless for metrology. Additionally, measurement sensitivity and optimal probe states depend on local Hamiltonians, while entanglement measures are independent of such operations. Finally, to further analyze the role of entanglement in metrology, consider a single mode state of the form[15]

$$|\Psi\rangle = \frac{|0\rangle + |N\rangle}{\sqrt{2}}\,, \tag{4}$$

[a]Feeding both the inputs of a Mach–Zehnder interferometer with vacuum squeezed along two orthogonal axes provides the Heisenberg limit of $1/N$. This is most easily understood as the outcome of having a two-mode squeezed state in the interferometer.[5,8]

that undergoes a dynamics given by $U_\phi = e^{-i\phi a^\dagger a}$. The state after the evolution is given by

$$|\Psi_\phi\rangle = \frac{|0\rangle + e^{-iN\phi}|N\rangle}{\sqrt{2}}, \tag{5}$$

and the measurement $M = |N\rangle\langle 0| + |0\rangle\langle N|$ allows us to estimate ϕ with a precision that scales as $1/N$ as in Eq. (3). We can therefore beat the SQL, and attain the Heisenberg limit without investing in the preparation of entangled states, but merely superpositions.[b] However, we do require a phase reference to perform the measurement M and indeed, a shared reference frame is a nontrivial resource, and its interconvertibility into and from quantum entanglement is an interesting question in itself.[16] It is therefore clear that some additional coherent resource is indeed necessary to beat the SQL, but that need not necessarily be entanglement. An interesting parallel is the Grover search algorithm that requires quantum superpositions but no entanglement in providing a square root improvement[17] in the unstructured database search problem. The connection between parameter estimation and database search, and the role of quantum superpositions in providing quadratic improvements is a curious one requiring further research.

An intriguing case-study for quantum enhancement in sensing is quantum illumination introduced by Lloyd.[18] The task is to infer the presence or absence of a weakly reflecting object nestled in a given region of space with a high temperature thermal bath by shining some light in the direction of the object and analyzing the light received from that direction. Lloyd's initial scheme suggested immense enhancements in distinguishing the two possibilities if one uses an entangled single-photon state as opposed to unentangled single-photon states.[18] This result was particularly fascinating because the high temperature bath and low reflectivity of the object results in a final state that has no entanglement at all. Thus, an initially entangled but eventually unentangled probe provides substantial quantum advantage. It was later shown that the performance of Lloyd's single-photon "quantum illumination" system is, at best, equal to that of a coherent-state transmitter of the same average photon number, and may be substantially worse.[19] In fact, in the low-noise regime, where entanglement depreciation is low, quantum illumination is unlikely to provide substantial improvement. However, in the high-loss regime when there is no entanglement, a more complete analysis using two-mode squeezed states that goes beyond the single-photon analysis, still shows some advantage.[20] The mysterious case of attaining a quantum advantage when entanglement is absent but not when entanglement is present makes the connection between quantum enhancements and entanglement rather tenuous.

[b]While the baryon number conservation forbids the preparation of superposition of particles with different masses such as atoms and ions, quantum states with superpositions of different photon numbers is possible.

Beyond unearthing the role of entanglement in providing quantum advantages in quantum metrology,[c] an additional, and vital question is the amount of advantage that quantum mechanics can provide. We will address both these issues in this review. Our discussion will revolve largely around the recent results in nonlinear quantum metrology.[23–35] Theoretical developments and experimental efforts have opened a new avenue for the development of quantum sensing, and provide a new workbench for exploring the questions raised above. In particular, we will discuss the role of nonlinear Hamiltonians in the estimation process *vis-a-vis* their potential of generating entanglement, beginning with probe states that are not entangled. We will discuss the progress in using systems with quadratic ground state Hamiltonians such as Bose–Einstein condensates (BECs) and cold atomic ensembles in quantum metrology.

2. Quantum Metrology

The single parameter estimation problem can be cast as the inference of a coupling parameter γ in the Hamiltonian

$$H_\gamma = \gamma H_0 \,, \tag{6}$$

by observing the evolution of a probe state under it. We take γ to have the units of frequency, whereby H_0 is a dimensionless coupling Hamiltonian and we work in units where $\hbar = 1$. The appropriate measure of the precision with which γ can be determined is the units-corrected mean-square deviation of the estimate $\gamma_{\rm est}$ from the true value γ[36,37]

$$\delta\gamma = \sqrt{\left\langle \left(\frac{\gamma_{\rm est}}{|d\langle\gamma_{\rm est}\rangle/d\gamma|} - \gamma \right)^2 \right\rangle} \,. \tag{7}$$

This estimator uncertainty is inversely proportional to the displacement in Hilbert space of the state of the probe corresponding to small changes in γ. The fundamental limit on the precision of parameter estimation, as an extension of classical estimation theory, is given by the quantum Cramér–Rao bound[36–39] as

$$\delta\gamma \geq \frac{1}{\sqrt{\nu}\, t\sqrt{\mathfrak{F}}} \geq \frac{1}{2\sqrt{\nu}\, t\langle\Delta H_0\rangle} \,, \tag{8}$$

where ν is the total number of interactions, each of duration t, between the system and the probe, $\mathfrak{F}$ is the quantum Fisher information of the initial state of the problem and $\langle\Delta H_0\rangle^2$ is the variance of H_0 with respect to the initial probe state. The quantum Fisher information (QFI) quantifies the amount of information about

[c]There have been suggestions of beating the SQL and even attaining the Heisenberg limit without the use of quantum entanglement.[21] However, it is known that shuttling a single probe through the system under query does require the maintenance of quantum coherence over an exponentially extended length of time,[22] and infact both the entangled, and entanglement-free protocols have equivalent communication complexity.

the unknown parameter that can get imprinted on the state of the quantum probe when it undergoes the parameter dependent evolution in Eq. (6). Since the probe is in itself a quantum system, there is the question of the readout of the state of the probe after the parameter dependent evolution so as to extract the information about the parameter. The readout is assumed to be such that the it maximizes the amount of information that is extracted. So the bound on the measurement precision becomes solely a function of the initial probe state and the dynamics it undergoes. The optimal readout on the probe always exists in the case of single parameter estimation, and is given by projective measurements on to the complete basis set furnished by the orthonormal eigenvectors of the symmetric logarithmic derivative operator.[36] The factor $1/\sqrt{\nu}$ is a purely classical statistical improvement coming from multiple runs of the experiment, and the Cramér–Rao bound for a single parameter can always be attained in the limit of asymptotically large ν. Increasing the interaction time t can also enhance precision, but it is often restricted in practical scenarios by decoherence or temporal fluctuations in γ. For a given H_0, the QFI is upper bounded by[25,36]

$$\sqrt{\mathfrak{F}} \leq 2\langle \Delta H_0 \rangle \leq \|H_0\| = (\lambda_{\rm M} - \lambda_{\rm m})\,, \tag{9}$$

where $\lambda_{\rm M}(\lambda_{\rm m})$ is the maximum (minimum) eigenvalue of H_0, $||\cdot||$ is an operator seminorm for Hermitian operators.[d] The inequalities in Eq. (9) are satisfied for a pure state of the form $(|\lambda_{\rm M}\rangle + e^{i\theta}|\lambda_{\rm m}\rangle)/\sqrt{2}$. Here $|\lambda_{\rm M}\rangle$ ($|\lambda_{\rm m}\rangle$) denote the eigenvectors of H_0 corresponding to its maximum (minimum) eigenvalue.

Now, consider a Hamiltonian of the form

$$H_0 = \sum_{\{j_1,\ldots,j_k\}} H^{(k)}_{j_1,\ldots,j_k}\,, \tag{10}$$

where k is the degree of multi-body coupling, and the sum is over all k-body subsystems. Assume that the k-body coupling $H^{(k)}$ is symmetric, and that the chosen k is the highest degree of coupling involving the parameter γ. In case there are lower order terms that include the same parameter, and those terms do not commute, an effective Hamiltonian and parameter can be obtained to which the theory of nonlinear quantum metrology can be applied. In general,[25]

$$||H_0|| \leq \sum_{\{j_1,\ldots,j_k\}} ||H^{(k)}_{j_1,\ldots,j_k}|| \leq \binom{N}{k}\, ||H^{(k)}|| \sim \frac{N^k}{k!}||H^{(k)}||\,, \tag{11}$$

where we have used the triangle inequality for the seminorm, the symmetry of the operator involved, and assumed that $k \ll N$, where N is the number of constituents in the quantum probe. In the special case when the multi-body interaction terms are products of single-body operators

$$H^{(k)}_{j_1,\ldots,j_k} = H_{j_1} \otimes \cdots \otimes H_{j_k}\,, \tag{12}$$

[d]There are cases, for instance in optical interferometry, where the maximum eigenvalue is unbounded. In that case, scaling can be framed in terms of the mean energy.

the semi-norm of the parameter independent part of the probe Hamiltonian reduces to

$$||H_0|| \sim \frac{N^k}{k!}(\lambda_{\rm M}^k - \lambda_{\rm m}^k)\,. \tag{13}$$

For $k = 1$, this leads to the Heisenberg limited scaling of $1/N$ for the measurement uncertainty. More generally, however, the limit attainable by quantum mechanics scales as $1/N^k$, and might more sensibly be labeled as the Heisenberg limit now.[e]

The result above is significant both theoretically and experimentally. It shows that the scaling of $1/N$, thought to be a universal, fundamental limit,[14] is not, but rather an instance of a more general result. In hindsight, as it often is, this particular generalization seems evident, since the precision of any estimate is governed by the evolution of the probe state under the Hamiltonian. Second, it allows for parameter estimation with an improved scaling given the same set of resources as quantified by N, which is the ultimate goal of metrology. This result also implies that quantum metrology using systems with nonlinear interactions such as BECs have the potential of providing estimates with higher precisions than those suggested by present experiments.[40] Recent studies of condensate systems from this perspective has lead to improved understanding of BECs and their evolution in highly anisotropic traps,[41] and further advances on these lines can be expected in the future.

Heuristically, the quantum limit in metrology can be thought of as being proportional to the number of commuting terms in the generating Hamiltonian. In other words, a quantum probe of the form $(|\lambda_{\rm M}\rangle^{\otimes N} + |\lambda_{\rm m}\rangle^{\otimes N})/\sqrt{2}$, under H_0 in Eqs. (10) and (12) evolves to $(|\lambda_{\rm M}\rangle^{\otimes N} + e^{iN^k\gamma}|\lambda_{\rm m}\rangle^{\otimes N})/\sqrt{2}$, and the enhanced relative phase picked up by the probe leads to the limit in Eq. (13). This limit of $1/N^k$ is always attainable, but might possibly require the preparation of an entangled state just described or one of the form in Eq. (4). Compared to the SQL of $1/\sqrt{N}$ introduced in Sec. 1, nonlinear dynamics appears to be able to provide a metrological enhancement greater than entanglement can provide, which is only a square root improvement. The caveat lies in the validity of the SQL under nonlinear evolutions. The scaling of the precision in an entirely classical scenario under nonlinear evolutions would be a fairer comparison to the $1/N^k$ scaling, and will be the subject of

[e]The phrase "Heisenberg limit" was first used explicitly by Holland and Burnett,[9] referring to the number-phase uncertainty associated with the Heisenberg uncertainty relation. The essence, however, was present in the early work of Caves[5] which uses nonclassical light to beat the SQL. Incidentally, the SQL is also a consequence of the Heisenberg uncertainty relations. Therefore, the excessive sanctity endowed on the phrase "Heisenberg limit" to denote the $1/N$ limit should be scrutinized more critically, with particular cognizance to the fact that it should label the ultimate scaling that quantum mechanics can provide in the precision of estimating a parameter as opposed to the best classical limit.

the next section. As we will see, for a broad class of Hamiltonians, the improvement is always quadratic.[f]

3. Quantum Metrology with Product States

In this section, we begin with a Hamiltonian of the form in Eq. (12), given by

$$H_0 = \left(\sum_{j=1}^{N} h_j\right)^k = \sum_{a_1,\ldots,a_k}^{N} h_{a_1}\cdots h_{a_k}\,, \tag{14}$$

where we have omitted the tensor products for brevity. Our aim is to derive lower bounds on $\delta\gamma$ in the situation where the initial state is a pure product state,[27]

$$|\Psi_0\rangle = |\psi_1\rangle \otimes \cdots \otimes |\psi_N\rangle\,. \tag{15}$$

We start from the state-dependent bound in Eq. (8) to evaluate ΔH_0. We begin by writing

$$H_0 = \sum_{(a_1,\ldots,a_k)} h_{a_1}\cdots h_{a_k} + \binom{k}{2} \sum_{(a_1,\ldots,a_{k-1})} h_{a_1}\cdots h_{a_{k-2}} h_{a_{k-1}}^2 + \cdots\,, \tag{16}$$

where a summing range with parentheses, $(a_1,\ldots,a_l)$, denotes a sum over all l-tuples with distinct elements. The two sums in Eq. (16) are the leading- and subleading-order terms in an expansion in which successive sums have fewer terms. The first sum in Eq. (16), in which the terms have no duplicate factors, has $N!/(N-k)! = \mathcal{O}(N^k)$ terms, and the second sum, in which one factor is duplicated in each term, has $N!/(N-k-1)! = \mathcal{O}(N^{k-1})$ terms. The binomial coefficient multiplying the second sum accounts for the number of ways of choosing the factor that is duplicated. The next sums in the expansion, involving terms with factors h_j^3 and $h_j^2 h_l^2$, have $N!/(N-k-2)! = \mathcal{O}(N^{k-2})$ terms. These expansions require that $N \geq k$, which we assume henceforth, and the scalings we identify further require that $N \gg k$.

Given the expansion in Eq. (16), the expectation value of H_0 has the form

$$\begin{aligned}\langle H_0\rangle = &\sum_{(a_1,\ldots,a_k)} \langle h_{a_1}\rangle\cdots\langle h_{a_k}\rangle + \binom{k}{2} \sum_{(a_1,\ldots,a_{k-1})} \langle h_{a_1}\rangle\cdots\langle h_{a_{k-2}}\rangle\langle h_{a_{k-1}}^2\rangle \\ &+ \mathcal{O}(N^{k-2})\,.\end{aligned} \tag{17}$$

[f]An exponential advantage in the scaling of the precision attainable in quantum metrology has been suggested,[42] and was in fact, the impetus behind the systematic study of nonlinear metrology.[25,27,28] The scheme requires N-body interactions, and every value of N would lead to a different coupling parameter to be estimated. The notion of asymptotic scaling of the precision in the limit of varying N is therefore not well defined.

The expression for $\langle H_0^2\rangle$ follows by replacing k with $2k$, as

$$\langle H_0^2\rangle = \sum_{(a_1,\ldots,a_{2k})} \langle h_{a_1}\rangle\cdots\langle h_{a_{2k}}\rangle + \binom{2k}{2} \sum_{(a_1,\ldots,a_{2k-1})} \langle h_{a_1}\rangle\cdots\langle h_{a_{2k-2}}\rangle\langle h_{a_{2k-1}}^2\rangle + \mathcal{O}(N^{2k-2})\,. \tag{18}$$

By changing the initial sum in Eq. (17) to an unrestricted sum, we can rewrite $\langle H_0\rangle$ to the required order as

$$\langle H_0\rangle = \sum_{a_1,\ldots,a_k} \langle h_{a_1}\rangle\cdots\langle h_{a_k}\rangle + \binom{k}{2} \sum_{(a_1,\ldots,a_{k-1})} \langle h_{a_1}\rangle\cdots\langle h_{a_{k-2}}\rangle\Delta h_{a_{k-1}}^2 + \mathcal{O}(N^{k-2})\,. \tag{19}$$

Squaring this expression and changing the unrestricted sums back to restricted ones, again keeping only the leading- and subleading-order terms, gives

$$\langle H_0\rangle^2 = \sum_{(a_1,\ldots,a_{2k})} \langle h_{a_1}\rangle\cdots\langle h_{a_{2k}}\rangle + \binom{2k}{2} \sum_{(a_1,\ldots,a_{2k-1})} \langle h_{a_1}\rangle\cdots\langle h_{a_{2k-2}}\rangle\langle h_{a_{2k-1}}\rangle^2 + 2\binom{k}{2} \sum_{(a_1,\ldots,a_{2k-1})} \langle h_{a_1}\rangle\cdots\langle h_{a_{2k-2}}\rangle\Delta h_{a_{k-1}}^2 + \mathcal{O}(N^{2k-2})\,. \tag{20}$$

We can now find $\langle\Delta H_0\rangle^2$ by subtracting Eq. (20) from Eq. (18)

$$\begin{aligned}\langle\Delta H_0\rangle^2 &= k^2 \sum_{(a_1,\ldots,a_{2k-1})} \langle h_{a_1}\rangle\cdots\langle h_{a_{2k-2}}\rangle\Delta h_{a_{k-1}}^2 + \mathcal{O}(N^{2k-2}) \\ &= k^2\left(\sum_{j=1}^N \langle h_j\rangle\right)^{2(k-1)}\left(\sum_{j=1}^N \Delta h_j^2\right) + \mathcal{O}(N^{2k-2})\,.\end{aligned} \tag{21}$$

In the final form, we take advantage of the fact that in the now leading-order sum, the restricted sum can be converted to an unrestricted one.

To make the QFI in Eq. (8) as large as possible, we maximize the variance $\langle\Delta H_0\rangle^2$ of Eq. (21). We can immediately see that for fixed expectation values $\langle h_j\rangle$, we should maximize the variances Δh_j^2, and this is done by using for each constituent a state that lies in the subspace spanned by $|\lambda_{\rm M}\rangle$ and $|\lambda_{\rm m}\rangle$. Letting p_j be the probability associated with $|\lambda_{\rm M}\rangle$ for the jth constituent, we have

$$\begin{aligned} x_j &\equiv \langle h_j\rangle = p_j\lambda_{\rm M} + (1-p_j)\lambda_{\rm m} = \lambda_{\rm m} + p_j\|h\|\,, \\ \langle\Delta h_j\rangle^2 &= p_j\lambda_{\rm M}^2 + (1-p_j)\lambda_{\rm m}^2 - x_j^2 = \|h\|^2 p_j(1-p_j) = (\lambda_{\rm M}-x_j)(x_j-\lambda_{\rm m})\,.\end{aligned} \tag{22}$$

Thus, we maximize

$$\langle\Delta H_0\rangle^2 = k^2\left(\sum_{j=1}^N x_j\right)^{2(k-1)} \sum_{j=1}^N (\lambda_{\rm M}-x_j)(x_j-\lambda_{\rm m}) \tag{23}$$

within the domain defined by $\lambda_{\rm m} \le x_j \le \lambda_{\rm M}$, $j = 1,\ldots,N$.

Besides $0 = \sum_j x_j$ which is a potential extremum of $\langle \Delta H_0 \rangle^2$, we find that the conditions for extrema of $\langle \Delta H_0 \rangle^2$ imply that $x_j = x$ (and thus $p_j = p$) for $j = 1, \ldots, N$. Thus, the optimal states in the initial product state in Eq. (15) have the form

$$|\psi_j\rangle = \sqrt{p}\,|\lambda_{\rm M}\rangle + e^{i\phi_j}\sqrt{1-p}\,|\lambda_{\rm m}\rangle\,. \tag{24}$$

The only possible difference between the states of the different constituents is in the relative phase between $|\lambda_{\rm M}\rangle$ and $|\lambda_{\rm m}\rangle$.

Since the optimal constituent states live and evolve in a two-dimensional subspace, we can regard the constituents effectively as qubits, with standard basis states $|0\rangle = |\lambda_{\rm M}\rangle$ and $|1\rangle = |\lambda_{\rm m}\rangle$, serving as the basis for constructing Pauli operators X, Y and Z. Restricted to this subspace, the operator h takes the form

$$h = \lambda_{\rm M}|0\rangle\langle 0| + \lambda_{\rm m}|1\rangle\langle 1| = \bar{\lambda}\mathbb{I} + \|h\|Z/2\,, \tag{25}$$

where $\bar{\lambda} \equiv (\lambda_{\rm M} + \lambda_{\rm m})/2$ is the arithmetic mean of the largest and smallest eigenvalues of h.

In the following, we assume that all the constituents have zero relative phase ($\phi_j = 0$), giving an initial state $|\Psi_\beta\rangle = |\psi_\beta\rangle^{\otimes n}$, where

$$|\psi_\beta\rangle = e^{-i\beta Y/2}|0\rangle = \cos(\beta/2)|0\rangle + \sin(\beta/2)|1\rangle\,, \tag{26}$$

with $p = \cos^2(\beta/2)$. The corresponding initial density operator is

$$\rho_\beta = |\Psi_\beta\rangle\langle\Psi_\beta| = \bigotimes_{j=1}^{N} \frac{1}{2}(\mathbb{I}_j + X_j \sin\beta + Z_j \cos\beta)\,. \tag{27}$$

The variance of H_0 now takes the simple form

$$\begin{aligned}\langle \Delta H_0 \rangle^2 &= k^2 N^{2k-1} \langle h \rangle^{2(k-1)} (\Delta h)^2 \\ &= k^2 N^{2k-1} x^{2(k-1)} (\lambda_{\rm M} - x)(x - \lambda_{\rm m})\,,\end{aligned} \tag{28}$$

which leads, via the QFI in Eq. (8), to a sensitivity that scales as $1/N^{k-1/2}$ for input product states. This should be compared with the $1/N^k$ scaling that can be obtained by using initial entangled states, as in Sec. 2. Notice that for $k = 1$, this reduces the SQL in Eq. (1). More importantly, for $k \geq 2$, the $1/N^{k-1/2}$ scaling is better than the $1/N$ scaling of the Heisenberg limit, which is the best that can be achieved in the $k = 1$ case even with entangled initial states.

3.1. *Optimal probe states and separable measurements*

The problem of finding the optimal input product state is now reduced to maximizing the $2k$-degree polynomial

$$\begin{aligned} f(x) &\equiv x^{2(k-1)}(\lambda_{\rm M} - x)(x - \lambda_{\rm m}) \\ &= x^{2(k-1)}\left(\|h\|^2/4 - (x - \bar{\lambda})^2\right)\end{aligned} \tag{29}$$

with respect to the single variable $x = \langle h \rangle$ on the domain $\lambda_{\rm m} \leq x \leq \lambda_{\rm M}$. The condition for an extremum is

$$0 = f'(x) = 2x^{2k-3}\big[(k-1)\big(\|h\|^2/4 - (x-\bar{\lambda})^2\big) - x(x-\bar{\lambda})\big]\,. \tag{30}$$

We assume $k \geq 2$, because the $k = 1$ case is already well understood with a single maximum at $x = \bar{\lambda}$, corresponding to equal probabilities for $|\lambda_{\rm M}\rangle$ and $|\lambda_{\rm m}\rangle$ and to $\langle \Delta H_0 \rangle^2 = N\|h\|^2/4$, as discussed earlier.

The polynomial f vanishes at $x = \lambda_{\rm m}, \lambda_{\rm M}$ and the form of the (nonzero) solutions of Eq. (30) is

$$x_\pm = \left(1 - \frac{1}{2k}\right)\bar{\lambda} \pm \frac{1}{2}\sqrt{\frac{\bar{\lambda}^2}{k^2} + \left(1 - \frac{1}{k}\right)\|h\|^2}\,. \tag{31}$$

As k increases, x_+ approaches $\lambda_{\rm M}$, and x_- approaches $\lambda_{\rm m}$. Indeed, as $k \to \infty$, we have $x_+ = (1 - 1/2k)\lambda_{\rm M}$, corresponding to $p_+ = 1 - \lambda_{\rm M}/2k\|h\|$ and $\langle \Delta H \rangle^2 = (k/2e)(n\lambda_{\rm M})^{2k-1}\|h\|$, and $x_- = (1 - 1/2k)\lambda_{\rm m}$, corresponding to $p_- = -\lambda_{\rm m}/2k\|h\|$ and $\langle \Delta H_0 \rangle^2 = (k/2e)(-N\lambda_{\rm m})^{2k-1}\|h\|$.

Another important limiting case occurs when $\lambda_{\rm m} = -\lambda_{\rm M}$. Then the maxima occur symmetrically at

$$x_\pm = \pm\frac{1}{2}\|h\|\sqrt{1 - 1/k}\,, \tag{32}$$

corresponding to probabilities $p_\pm = \frac{1}{2} + x_\pm/\|h\| = \frac{1}{2}(1 \pm \sqrt{1 - 1/k}) = 1 - p_\mp$ and to

$$\sin\beta_\pm = \sqrt{1/k}. \tag{33}$$

The two maxima lead to the same variance, and a QFI of

$$\langle \Delta H_0 \rangle^2 = k(1 - 1/k)^{k-1}N^{2k-1}(\|h\|/2)^{2k}\,, \tag{34}$$

thus yielding a precision scaling of

$$\delta\gamma \geq \frac{2^{k-1}}{k^{1/2}(1 - 1/k)^{(k-1)/2}}\,\frac{1}{t\,N^{k-1/2}\|h\|^k}\,. \tag{35}$$

Of course, when $\lambda_{\rm m} = -\lambda_{\rm M}$, we can always choose units such that $\lambda_{\rm M} = 1/2$ ($\|h\| = 1$), which means that the single-body operators are $h_j = Z_j/2$. It is this situation that we analyze in the remainder of this section, for $k = 2$, in which case

$$\delta\gamma \geq \frac{2}{t\,N^{3/2}}\,. \tag{36}$$

We now consider the special case in which the single-body operators are $h_j = Z_j/2$, leading to a coupling Hamiltonian

$$H = \left(\sum_j Z_j/2\right)^k = J_z^k\,. \tag{37}$$

We introduce J_z as the z component of a "total angular momentum" corresponding to the effective qubits. We assume an initial state of the form Eq. (27), and we let this state evolve for a very short time, i.e. $\phi \equiv \gamma t \ll 1$. After the time evolution, we measure the separable observable

$$J_y = \sum_j Y_j \,. \tag{38}$$

Over ν trials, we estimate γ as a scaled arithmetic mean of the results of the J_y measurements.

The expectation value of any observable at time t is given by

$$\langle M\rangle_t = \mathrm{Tr}\left(U^\dagger M U \rho_\beta\right) = \langle U^\dagger M U\rangle \,, \tag{39}$$

where $U = e^{-iH_\gamma t} = e^{-iH\phi}$, and where we introduce the convention that an expectation value with no subscript is taken with respect to the initial state. For small ϕ, we have

$$U^\dagger M U = M - i\phi[M, H] + \mathcal{O}(\phi^2) \,. \tag{40}$$

Thus, the expectation value and variance of J_y at time t take the form

$$\langle J_y\rangle_t = \langle J_y\rangle - i\phi\langle[J_y, H]\rangle + \mathcal{O}(\phi^2) \,, \tag{41a}$$

$$(\Delta J_y)_t^2 = (\Delta J_y)_0^2 - i\phi\big\langle(J_y - \langle J_y\rangle)[J_y, H] + [J_y, H](J_y - \langle J_y\rangle)\big\rangle + \mathcal{O}(\phi^2) \,. \tag{41b}$$

The initial expectation value and variance of J_y are those of an angular-momentum coherent state in the x–z plane:

$$\langle J_y\rangle = 0 \,, \tag{42a}$$

$$(\Delta J_y)_0^2 = \langle J_y^2\rangle = \frac{1}{4}\sum_{j,l}\langle Y_j Y_l\rangle = \frac{N}{4} \,. \tag{42b}$$

In evaluating the other expectation values in Eqs. (41), we can use the expressions from earlier in the section, since we are only interested in the leading-order behavior in n. To leading order, the coupling Hamiltonian has the form

$$H = \frac{1}{2^k}\sum_{(a_1,\ldots,a_k)} Z_{a_1}\cdots Z_{a_k} + \mathcal{O}(N^{k-1}) \,. \tag{43}$$

Here we use $\approx$ to indicate equalities that are good to leading order in N. We can now write

$$\begin{aligned}
[J_y, H] &\approx \frac{1}{2^{k+1}}\sum_{j=1}^{N}\sum_{(a_1,\ldots,a_k)}[Y_j, Z_{a_1}\cdots Z_{a_k}] \\
&= \frac{i}{2^k}\sum_{l=1}^{k}\sum_{(a_1,\ldots,a_k)} Z_{a_1}\cdots Z_{a_{l-1}} X_{a_l} Z_{a_{l+1}}\cdots Z_{a_k} \\
&= \frac{ik}{2^k}\sum_{(a_1,\ldots,a_k)} X_{a_1} Z_{a_2}\cdots Z_{a_k} \,,
\end{aligned} \tag{44}$$

from which it follows that

$$\langle [J_y, H] \rangle \approx \frac{ik}{2^k} \sum_{(a_1,\ldots,a_k)} \langle X_{a_1} \rangle \langle Z_{a_2} \rangle \cdots \langle Z_{a_k} \rangle$$

$$\approx ik \langle J_x \rangle \langle J_z \rangle^{k-1} . \tag{45}$$

This procedure can be extended one step further to show that to leading order in N, the expectation of the terms of $\mathcal{O}(\phi^2)$ Eq. (41b) vanishes. Our results to this point are

$$\langle J_y \rangle_t \approx \phi k \langle J_x \rangle \langle J_z \rangle^{k-1} + \mathcal{O}(\phi^2)$$

$$= \phi k (N/2)^k \sin\beta \cos^{k-1}\beta + \mathcal{O}(\phi^2) , \tag{46a}$$

$$(\Delta J_y)_t \approx \sqrt{N}/2 + \mathcal{O}(\phi^2) . \tag{46b}$$

If we let our estimator ϕ_{est} be the arithmetic mean of the ν measurements of J_y, scaled by the factor $(d\langle J_y \rangle_t / d\phi)^{-1} = 1/k(N/2)^k \sin\beta \cos^{k-1}\beta$, we have

$$\langle \phi_{\text{est}} \rangle = \frac{\langle J_y \rangle_t}{d\langle J_y \rangle_t / d\phi} \approx \phi + \mathcal{O}(\phi^2) , \tag{47}$$

$$\delta\phi \approx \frac{1}{\sqrt{\nu}} \frac{(\Delta J_y)_t}{|d\langle J_y \rangle_t / d\phi|} + \mathcal{O}(\phi)$$

$$\approx \frac{1}{\sqrt{\nu}} \frac{2^{k-1}}{kN^{k-1/2} \sin\beta |\cos^{k-1}\beta|} + \mathcal{O}(\phi) . \tag{48}$$

This scheme thus attains the $\mathcal{O}(N^{-k+1/2})$ scaling that is the best that can be achieved by initial product states. Moreover, the minimum of $\delta\phi$, occurring when $\sin\beta = \sqrt{1/k}$, gives an optimal sensitivity of

$$\delta\phi \approx \frac{1}{\sqrt{\nu}} \frac{2^{k-1}}{k^{1/2}(1-1/k)^{(k-1)/2}} \frac{1}{N^{k-1/2}} + \mathcal{O}(\phi) . \tag{49}$$

For $k = 2$, the two optimal values of β are $\beta = \pi/4$ and $\beta = 3\pi/4$, and the sensitivity becomes

$$\delta\gamma \approx \frac{1}{t\sqrt{\nu}} \frac{2}{N^{3/2}} + \mathcal{O}(\phi) , \tag{50}$$

in harmony with results obtained earlier in Eqs. (35) and (36).

Aside from showing that the optimal scaling for initial product states can be achieved, the analysis above illustrates how the product-state scheme works in a regime that has a very simple description. The J_z^k coupling Hamiltonian induces a nonlinear rotation about the z-axis, which rotates the state of the probe through an angle $\langle J_y \rangle_t / \langle J_x \rangle \approx \phi k \langle J_z \rangle^{k-1}$. This rotation induces a signal in J_y of size $\approx \phi k \langle J_x \rangle \langle J_z \rangle^{k-1}$, which is $k\langle J_z \rangle^{k-1}$ times bigger than for $k = 1$, and can be detected against the same coherent-state uncertainty $\sqrt{N}/2$ in J_y as for $k = 1$. To take advantage of the nonlinear rotation, we cannot make the J_x lever arm of

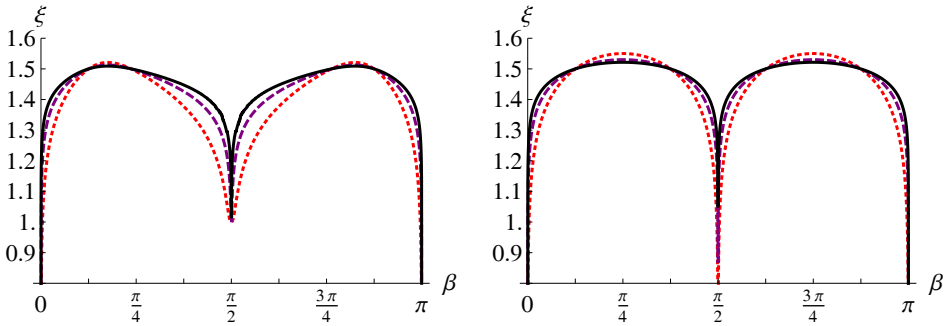

Fig. 1. Left: Scaling exponent ξ for J_x measurements. Right: Scaling exponent ξ for J_y measurements. The dotted (red) line is for $J = 10^3$, the dashed (purple) line for $J = 10^5$, and the solid (black) line for $J = 10^7$.

the rotation as large as possible, because the nonlinear rotation vanishes when the initial coherent state lies in the equatorial plane. Nonetheless, we still win when we make the optimal compromise between the nonlinear rotation and the lever arm. The optimal compromise comes from maximizing $\langle J_x\rangle\langle J_z\rangle^{k-1}$, which turns out to be exactly the same as finding the optimum in the QFI analysis of Sec. 3.1 because $\langle X\rangle = \sin\beta = \Delta Z$.

A more careful consideration of the terms neglected in this analysis suggests that, as formulated in this section, the small-time approximation requires that $\phi \ll 1/N^{k-1}$. Nonetheless, the analysis is consistent because ϕ can be resolved more finely than this scale, i.e. $\delta\phi\, N^{k-1} = \mathcal{O}(1/\sqrt{N})$. This conclusion is confirmed by the more detailed analysis[27] of the $k = 2$ case, which also shows that the simple model of the evolution of the spin-coherent state $e^{iJ_y\beta}|0\rangle^{\otimes N} = |\psi_\beta\rangle^{\otimes N}$, can be extended to much larger times.

To gain further insight into the scaling behavior, we plot the scaling exponent ξ in $\delta\phi = \mathcal{O}(n^{-\xi})$ as a function of β for J_x and J_y measurements (Fig. 1), using three very large values of J. For J_y measurements we calculate ξ at the optimal operating point, $\phi = 0$. The main differences between J_x and J_y measurements are the following: (i) right at $\beta = \pi/2$, J_x measurements have a scaling exponent of 1, whereas J_y measurements provide no information about γ; (ii) for J_y measurements, the plot of scaling exponent has two humps, nearly symmetric about $\beta = \pi/4$ and $\beta = 3\pi/4$, whereas for J_x measurements, the scaling exponent is better on the outside of the humps. The overall trend is for both measurements to have a scaling exponent of $\xi = 3/2$ in the limit of large J, except at $\beta = 0$, $\pi/2$, and π.

3.2. *Quantum metrology without entanglement*

The restriction to small values of ϕ in the above analysis is to ensure the attainability of the QFI using separable measurements such as J_x or J_y. For longer times, the phase dispersion in the spin-coherent state following the evolution under a nonlinear Hamiltonian leads to entangled states. One might however think that the

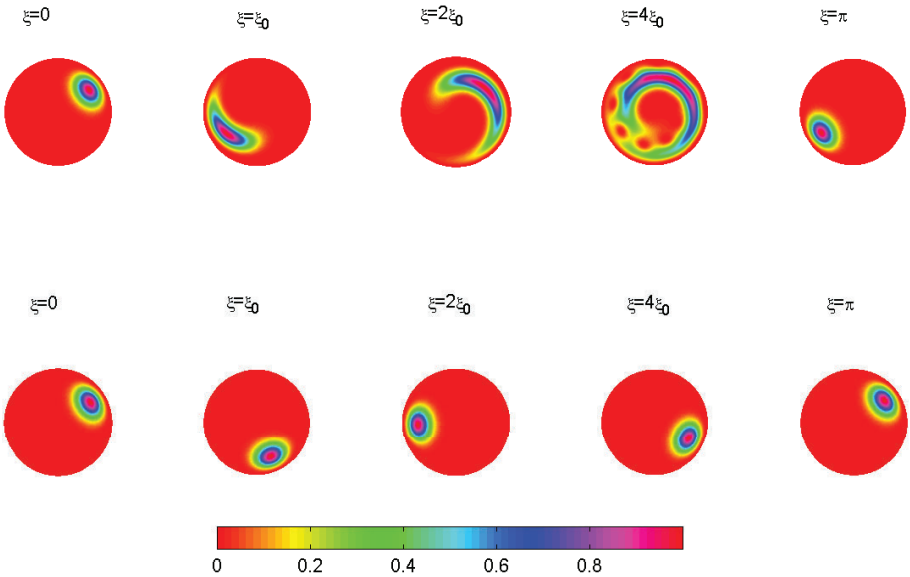

Fig. 2. Q-function for the evolution of a spin-coherent state under the Hamiltonian. Top: J_z^2. Bottom: nJ_z. The entanglement and phase dispersion in the top figure is a limitation to attaining the QFI using separable measurements for longer times.

entanglement generated under this evolution is the resource that leads to the enhanced precision of $1/N^{k-1/2}$. The realization to be made is that we would obtain exactly the same scaling if we evolved the initial spin-coherent state under the Hamiltonian $N^{k-1}J_z$. This Hamiltonian will generate no phase dispersion or entanglement, and we can attain the QFI using separable measurements. The comparison between the Q-function under the two different Hamiltonians for $k = 2$ is shown in Fig. 2.

With a $N^{k-1}J_z$ interaction, the optimal initial product state is $e^{-iJ_y\pi/2}|0\rangle^{\otimes N} = [(|0\rangle + |1\rangle)/\sqrt{2}]^{\otimes N}$. The state remains unentangled at all times, evolving to $[(e^{-i\gamma t N^{k-1}/2}|0\rangle + e^{i\gamma t N^{k-1}/2}|1\rangle)/\sqrt{2}]^{\otimes N}$. A measurement of J_x at time t has expectation value $\langle J_x\rangle = \frac{1}{2}N\cos(\gamma t N^{k-1})$ and uncertainty $\Delta J_x = \frac{1}{2}\sqrt{N}|\sin(\gamma t N^{k-1})|$, leading to a measurement precision $\delta\gamma = \Delta J_x/\sqrt{\nu}\,|d\langle J_x\rangle/d\gamma| = 1/tN^{k-1/2}\sqrt{\nu}$ after ν trials. A measurement of any other equatorial component of $\boldsymbol{J}$ achieves the same sensitivity. The enhanced scaling in a protocol that uses an $N^{k-1}J_z$ coupling and an initial product state is clearly due to the dynamics alone, not to entanglement of the constituent qubits. These results indicate that in quantum metrology, entanglement is important only in providing an optimal initial state, which leads to an improvement by a factor of $1/N^{1/2}$ over initial product states.

Physically, an $N^{k-1}J_z$ coupling cannot arise fundamentally as a *linear* coupling since the coupling strength would then depend on the number of constituents in the probe. However, for $k = 2$, we will now show that such a term can actually be

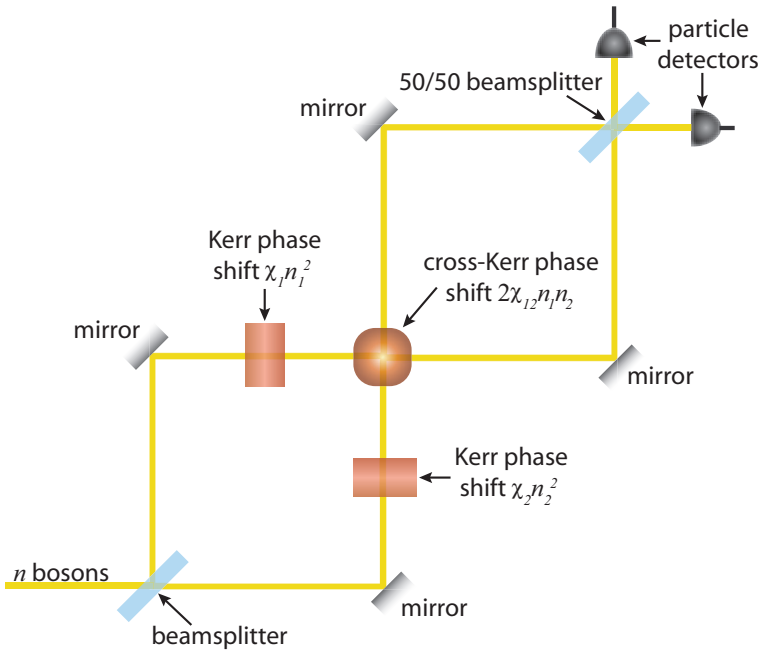

Fig. 3. Mach–Zehnder interferometer involving most general two-body interactions.[28]

arrived at naturally. The most general such Hamiltonian is

$$\mathcal{H}t/\hbar = \chi_1 N_1^2 + \chi_2 N_2^2 + 2\chi_{12} N_1 N_2 \,, \tag{51}$$

in systems of bosons that can occupy two modes with creation operators $a_1^\dagger$ and $a_2^\dagger$. In the Schwinger representation, with $J_z = \frac{1}{2}(N_1 - N_2)$ and $N = N_1 + N_2$, where $N_1 = a_1^\dagger a_1$ and $N_2 = a_2^\dagger a_2$ are the numbers of particles in the two modes. The bosons we consider interact with one another, but the interactions conserve particle number, so the system has a nonzero chemical potential. Our measurement protocols, for both types of coupling, can be represented in terms of the interferometer with nonlinear phase shifters depicted in Fig. 3. In terms of the Schwinger operators,

$$\mathcal{H}t/\hbar = (\chi + \chi_{12})N^2/2 + (\chi_1 - \chi_2)NJ_z + 2(\chi - \chi_{12})J_z^2 \,, \tag{52}$$

where $\chi = \frac{1}{2}(\chi_1 + \chi_2)$ is the average Kerr phase shift. The first term produces an overall phase shift and can be ignored. The NJ_z coupling comes from having different Kerr phase shifters in the two arms; to eliminate the J_z^2 interaction requires a cross-Kerr coupling $\chi_{12} = \chi$. Under these circumstances, we have $\mathcal{H} = \hbar\gamma N J_z$, with $\gamma t = \chi_1 - \chi_2$.

Having proven that it is possible to beat the SQL without investing in the preparation of fragile and complicated entangled states, in the next section, we present a proposal of implementing such a scheme. It involves two-mode BECs of

a very well-studied species, and we will consider their physics in the next section. We will also discuss the first experimental demonstration of beating the SQL and the $1/N$ limit using light-matter interfaces.

4. Experimental Systems for Nonlinear Quantum Metrology

Any physical system possessing a nonlinear Hamiltonian can be envisaged to implement the theoretical scheme outlined above. They include Bose–Einstein condensates (BECs), resonantly and off-resonantly coupled atomic ensembles with light, trapped ions and light in optical fibers. All these systems have been extensively studied in in their own right, and in the context of quantum information science. Some have, in fact, been used as test beds of quantum metrology as well. In this section, we first describe in some detail how the scheme proposed above can be implemented in a system of two-mode BECs. We then describe a recent experiment using light-matter interactions that has demonstrated the enhanced precision in the laboratory.

4.1. *Bose–Einstein condensates*

We consider a BEC of $N \gg 1$ atoms that can occupy two hyperfine states, henceforth labeled $|1\rangle$ and $|2\rangle$. We assume the BEC is at zero temperature and that all the atoms are initially condensed in state $|1\rangle$ with wave function $\psi_N(\mathbf{r})$, which is the N-dependent solution (normalized to unity) of the time-independent Gross–Pitaevskii equation[43–45]

$$\left(-\frac{\hbar^2}{2m}\nabla^2 + V(\mathbf{r}) + g_{11}N|\psi_N(\mathbf{r})|^2\right)\psi_N(\mathbf{r}) = \mu_N\psi_N(\mathbf{r})\,, \tag{53}$$

where $V(\mathbf{r})$ is the trapping potential, μ_N is the chemical potential, and g_{11} is the intraspecies scattering coefficient. This coefficient is determined by the s-wave scattering length a_{11} and the atomic mass m according to the formula $g_{11} = 4\pi\hbar^2 a_{11}/m$. A detailed discussion on quantum interferometry using BECs has recently presented by Lee *et al.*[46]

We describe the system by the so-called Josephson approximation, which assumes that both modes have and retain the same spatial wave function $\psi_N(\mathbf{r})$ from Eq. (53). In this approximation, the BEC dynamics is governed by the two-mode Hamiltonian

$$\hat{H} = NE_0 + \frac{1}{2}\eta_N \sum_{\alpha,\beta=1}^{2} g_{\alpha\beta}\hat{a}_\beta^\dagger\hat{a}_\alpha^\dagger\hat{a}_\alpha\hat{a}_\beta\,. \tag{54}$$

Here, $\hat{a}_\alpha^\dagger$ ($\hat{a}_\alpha$) creates (annihilates) an atom in the hyperfine state $|\alpha\rangle$, with wave function ψ_N, $g_{\alpha\beta} = 4\pi\hbar^2 a_{\alpha\beta}/m$, E_0 is the mean-field single-particle energy, given by

$$E_0 = \int d^3r \left(\frac{\hbar^2}{2m}|\nabla\psi_N|^2 + V(\mathbf{r})|\psi_N|^2\right), \tag{55}$$

and the quantity

$$\eta_N = \int d^3r |\psi_N(\mathbf{r})|^4 \tag{56}$$

is a measure of the inverse volume occupied by the condensate wave function ψ_N. Notice that this effective volume renormalizes the scattering interactions, thereby defining effective nonlinear coupling strengths $g_{\alpha\beta}\eta_N$. The Josephson approximation applies if one can drive fast transitions between the two hyperfine levels, the two levels are trapped by the same external potential, the atoms only undergo elastic collisions, and the spatial dynamics are slow compared to the accumulation of phases in the two hyperfine levels. In addition, notice that the zero-temperature mean-field treatment of the Josephson Hamiltonian in Eq. (54) assumes that the quantum depletion of the condensate is negligible. We make this assumption throughout on the grounds that the depletion is expected to be very small.[45]

Using the Schwinger angular-momentum operators, the Josephson-approximation evolution in Eq. (54) can be written as[43]

$$\hat{H} = \gamma_1 \eta_N N \hat{J}_z + \gamma_2 \eta_N \hat{J}_z^2 \,, \tag{57}$$

where we define two new coupling constants that characterize the interaction of the two modes,

$$\gamma_1 = \frac{1}{2}(g_{11} - g_{22}) \quad \text{and} \quad \gamma_2 = \frac{1}{2}(g_{11} + g_{22}) - g_{12} \,. \tag{58}$$

We omit *c-number* terms whose only effect is to introduce an overall global phase.

The dynamics governed by Eq. (57) is *almost* identical to that of an interferometer with nonlinear phase shifters as in Eq. (52). Due to the different scattering interactions, the first term of Eq. (57) introduces a relative phase shift that is proportional to the total number of atoms in the condensate, whereas the $\hat{J}_z^2$ term leads to more complicated dynamics that create entanglement and phase diffusion. Both terms can be used to implement nonlinear metrology protocols whose phase detection sensitivity scales better than $1/N$. For initial product states, the entanglement created by $\hat{J}_z^2$ has no influence on the enhanced scaling and therefore offers no advantage over the $N\hat{J}_z$ evolution. On the contrary, it is better to avoid the associated phase dispersion, and we next show how this works.

Suppose the first optical pulse puts each atom in a superposition $c_1|1\rangle + c_2|2\rangle$, where c_1 and c_2 can be assumed to be real (i.e. the first optical pulse performs a rotation about the y axis of the Bloch sphere). For short times, we can make a linear approximation to $\hat{J}_z^2$ in the Josephson Hamiltonian; i.e. we can set $\hat{J}_z^2 = (\langle \hat{J}_z \rangle + \Delta \hat{J}_z)^2 \simeq \langle \hat{J}_z \rangle^2 + 2\langle \hat{J}_z \rangle \Delta \hat{J}_z$, with $\langle \hat{J}_z \rangle = N(c_1^2 - c_2^2)/2$. The linear approximation amounts to neglecting the phase dispersion and corresponding entanglement produced by the $\hat{J}_z^2$ term. We need not make any such short-time approximation for the $N\hat{J}_z$ term. Up to irrelevant phases, the resulting evolution is a rotation of each atom's state about the z-axis of the Bloch sphere with angular

velocity

$$\Omega_N \equiv \frac{N\eta_N}{\hbar}[\gamma_1 + (c_1^2 - c_2^2)\gamma_2]. \tag{59}$$

Under these circumstances, the BEC acts like a linear Ramsey interferometer whose rotation rate is enhanced by a factor of $N\eta_N$, leading to a sensitivity that scales as $1/\sqrt{N}N\eta_N \simeq 1/N^{3/2}\eta_N$. If $\gamma_2 = 0$, the optimal initial state has $c_1 = c_2 = 1/\sqrt{2}$, but if $\gamma_1 = 0$, the optimal choice is $c_1 = \cos(\pi/8)$ and $c_2 = \sin(\pi/8)$, as in Eq. (33).

Achieving a $1/N^{3/2}$ scaling requires that η_N have no dependence on N. As noted above, however, η_N^{-1} is a measure of the volume occupied by the ground state wave function ψ_N. As atoms are added to a BEC, the wave function spreads because of the repulsive scattering of the atoms, thereby reducing η_N as N increases. To pin down how the measurement accuracy scales with N, we need to determine how η_N behaves as a function of N.

4.2. *Renormalization of the nonlinear interaction terms*

In a BEC, the trapping potential and the interatomic scattering competing forces that provides the equlibrium. The trap tries to bring the atoms together, thereby reducing the size of the atomic cloud while the scattering tends to spread out the cloud of atoms. Since all the atoms in the BEC share the same spatial wave function, the scattering term effectively spreads out the condensate wave function ψ_N. Strategies for compensating for the renormalization of the nonlinear interaction terms arising due to the spreading out of the BEC wave function as a function of N include using tighter traps and working with BECs confined to less than three dimensions. Anticipating these results, we compute the effect of η_N on the measurement accuracy assuming that the BEC is in d-dimensional space and that the trapping potential has the generic form

$$V(\mathbf{r}) = \frac{1}{2}kr^q \tag{60}$$

with even q. We have assumed here that the trap is spherically symmetric for simplicity and extensions to asymmetric traps is quite straightforward.

The large N limit for BECs is the Thomas–Fermi limit where we can ignore the kinetic term in the Hamiltonian. Then,[43–45]

$$|\psi_N(\mathbf{r})|^2 = \frac{\mu - V(\mathbf{r})}{gN}\,, \tag{61}$$

where μ is the chemical potential and $g = g_{11} + g_{22} + 2g_{12}$ for the the two mode BEC assuming that atoms in both internal states have the same form for the spatial parts of their wave functions. Since $|\psi_N(\mathbf{r})|^2$ must be positive, the radial extent of a BEC in a spherically symmetric potential is bounded from above by R such that

$$\mu = \frac{1}{2}kR^q\,. \tag{62}$$

The normalization of the single particle wave function yields

$$1 = \int |\psi_N(\mathbf{r})|^2 d\mathbf{r} = \frac{k}{2gN} \int d\Omega \int_0^R (R^q - r^q) r^{d-1} dr$$
$$= \frac{k}{2qN} R^{q+d} S_{d-1} \left(\frac{1}{d} - \frac{1}{q+d} \right), \tag{63}$$

where S_{d-1} is the surface area of the $d-1$ sphere with unit radius. For the cases that we are interested in, namely, for one, two and three dimensions, S_{d-1} takes on values 1, 2π and 4π, respectively. We can find R as a function of N from Eq. (63) and substitute it in Eqs. (62) and (61) to obtain

$$\eta = \frac{1}{g^2 N^2} \int (\mu - V(\mathbf{r}))^2 d^d r$$
$$= \left(\frac{kq}{g} \right)^{2-\frac{1}{d+q}} \left(\frac{S_{d-1}}{2d(d+q)} \right)^{1-\frac{1}{d+q}} \frac{1}{d+2q} N^{-\frac{d}{d+q}} \equiv \alpha_{d,q} N^{-\frac{d}{d+q}} . \tag{64}$$

The effective N dependence in the measurement uncertainties in γ_1 and γ_2 will scale as

$$\delta\gamma_{1,2} \sim \frac{1}{N^{\frac{3}{2}-\frac{d}{d+q}}} = \frac{1}{N^{\frac{d+3q}{2(d+q)}}} . \tag{65}$$

The exponent of N in $\delta\gamma_{1,2}$ is shown as a function of q for the one, two and three dimensional cases are shown in Fig. 4 (left). For a BEC in three dimensions contained within a harmonic trapping potential, $\delta\gamma \sim 1/N^{9/10}$ which is worse than the $1/N$ scaling. So either we have to use a trapping potential that confines the atoms more strongly than the harmonic potential or else work with BECs in less than three dimensions. In two dimensions, the performance with a BEC trapped in a harmonic potential will match the $1/N$ scaling and a one-dimensional BEC will better this scaling. In the limit of infinitely hard traps $q \to \infty$, the scaling

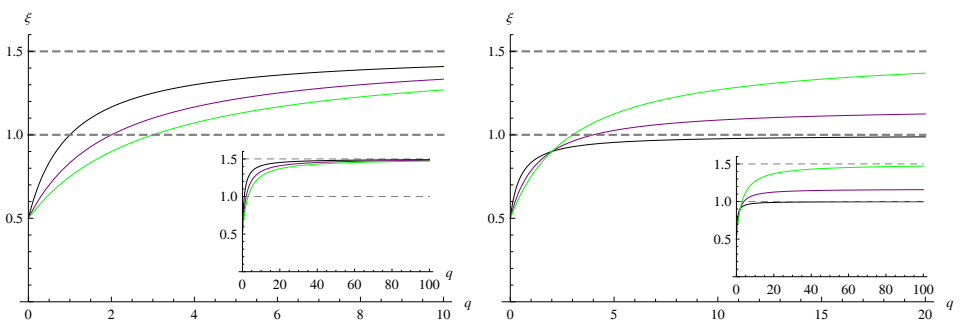

Fig. 4. (Color online) Left: The exponent of the scaling with N of the measurement uncertainty is shown as a function of the exponent of r in $V(\mathbf{r})$. One dimension (black), two dimensions (purple), and three dimensions (green). Right: one loose dimension (black), two loose dimensions (purple), and three loose dimensions (green).

attains the maximum possible value, as the shape and size of the wave function is independent of the number of atoms involved.

Since lower dimensional condensates offer better scaling due to the suppression of the N-dependence of η_N by constraining the BEC within a hard-walled trap so that it cannot expand as more atoms are added. BECs effectively confined to two or one dimensions and held in power-law trapping potentials along these dimensions are the sort found in real experiments. Thus, we look at the dependence of η_N on N for a BEC that is *loosely* trapped in d dimensions, referred to as *longitudinal* (L) dimensions, and *tightly* trapped in $D = 3 - d$ dimensions, referred to as *transverse* (T) dimensions. We assume that in the longitudinal dimensions, the atoms are trapped in a power-law potential as in Eq. (60) and that in the transverse dimensions, the trapping potential is harmonic,

$$V_T(\boldsymbol{\rho}) = \frac{1}{2} m\omega_T^2 \rho^2 \,. \tag{66}$$

The parameter q characterizes the hardness of the longitudinal trapping potential. We deal with a 3D trap by setting $D = 0$, meaning there are no transverse dimensions.

When N is small, the mean-field scattering energy is negligible compared to the atomic kinetic energy of the atoms and the trapping potential energy. In this situation, the scattering term in the GP equation can be neglected, and the ground state wave function is the solution of the Schrödinger equation for the trapping potential $V_L(\mathbf{r}) + V_T(\boldsymbol{\rho})$. As more atoms are added to the BEC, the repulsive scattering term in Eq. (53) comes into play and causes the wave function to spread. The two critical atom numbers, N_L and N_T, characterize the onset of spreading in the longitudinal and transverse dimensions. The lower critical atom number, N_L, is defined as the atom number at which the scattering term in the GP equation is as large as the longitudinal kinetic-energy term and thus characterizes when the wave function begins to spread in the longitudinal dimensions. The upper critical atom number, N_T, is defined as the atom number at which the scattering term is as large as the transverse kinetic energy and thus characterizes when the wave function begins also to spread in the transverse dimensions. The notion of an upper critical atom number only makes sense for 1D and 2D traps and not for $d = 3$.

The scaling in estimating the uncertainties of $\gamma_{1,2}$ is given by

$$\delta\gamma_{1,2} \sim \frac{1}{\sqrt{N} N \eta_N} \sim \frac{1}{N^{\xi}}, \tag{67}$$

and is provided in Table 1 in the different regimes. The critical numbers $N_{L,T}$ are governed by three length scales — the half-widths of the traps in the two directions, and the scattering length, and values for a typical implementation using ^{87}Rb condensates are known.[31,32] We next discuss some of the aspects of this implementation.

Table 1. Precision scaling in different regimes of atom numbers, plotted in Fig. 4.

	$N \ll N_L$	$N_L \ll N \ll N_T$	$N_T \ll N$
ξ	$\frac{3}{2}$	$\frac{d+3q}{2(d+q)}$	$\frac{3}{2} - \frac{3-d+2d/q}{5-d+2d/q}$

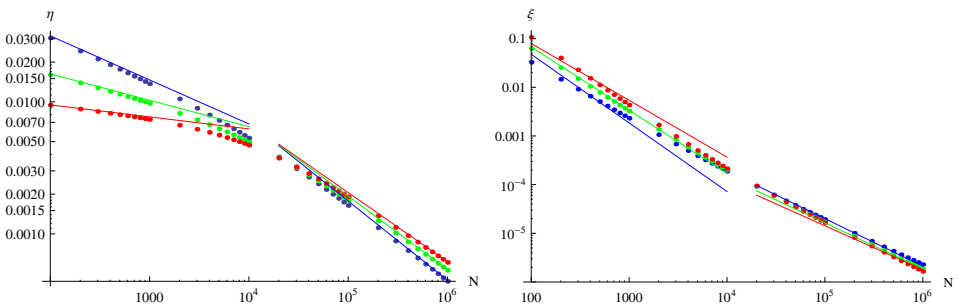

Fig. 5. (Color online) Left: The scaling of η with different condensate sizes and geometries. Right: The scaling of ξ with different condensate sizes and geometries, with $q = 2$ (blue), $q = 4$ (green), and $q = 10$ (red).

4.3. *Nonlinear metrology using ^{87}Rb condensates*

A good candidate for implementing the generalized metrology protocol is a BEC made of ^{87}Rb atoms constrained to the hyperfine levels $|F = 1, M_F = -1\rangle \equiv |1\rangle$ and $|F = 2, M_F = 1\rangle \equiv |2\rangle$. These states possess scattering properties that offer a natural way to suppress the phase diffusion introduced by the $\hat{J}_z^2$ evolution; namely, the s-wave scattering lengths for the processes $|1\rangle|1\rangle \to |1\rangle|1\rangle$, $|1\rangle|2\rangle \to |1\rangle|2\rangle$, and $|2\rangle|2\rangle \to |2\rangle|2\rangle$, respectively, are $a_{11} = 100.40a_0$, $a_{12} = 97.66a_0$, and $a_{22} = 95.00a_0$,[47] with a_0 being the Bohr radius, which implies that $\gamma_2 \simeq 0$. Consequently, the J_z^2 term becomes negligible, and the effective dynamics is simply described by the NJ_z coupling.

Numerical simulations for different trap geometries are presented in Fig. 5. For these simulations, the transverse frequency is set to 350 Hz and the longitudinal frequency to 3.5 Hz for the harmonic case ($q = 2$), with the result that the rescaled critical number in anisotropic traps $\bar{N}_T \simeq 14{,}000$ atoms. To compare the simulations for the different power-law potentials, we choose the stiffness parameter k so that $\bar{N}_T$ remains the same for the two other values of q. All the traps thus have the same one-dimensional regime of atom numbers. For such choice of parameters, we find $\rho_0 \simeq 0.6\,\mu$m and the aspect ratio of the traps (ρ_0:z_0) to be approximately equal to 1:10, 1:24, and 1:57, respectively, for $q = 2, 4, 10$. In addition, when $N = \bar{N}_T$, the condensate aspect ratios (ρ_0:z_N) are $1 : 158, 1 : 146$, and $1 : 138$ (for $q = 2, 4, 10$), parameters typical in elongated BECs.[48]

The above studies show that it is entirely feasible to beat the $1/N$ limit using two-mode BECs. In a BEC, the most significant loss channel is three-body losses. For two-mode BECs, there are other mechanisms, such as inelastic two-atom spin-exchange collisions. Simple analysis shows that there is a ratio of about 20 between the coherent and the loss mechanisms. It is also helpful that the optimal states and measurements are products, since loss of atoms does not lead to any loss of coherence. Of course, the number of atoms in a condensates is known to a finite precision. In particular, the number of atoms is not fixed from trial to trial. The variance in the measurement is typically of order $\sqrt{N}$, which is also the typical precision of atom numbers in BECs.[31] The time over which the experiment can be carried out is also limited by the implicit assumption that the two hyperfine species share the same spatial wave function is true only for short times, which is however enough to run our metrology scheme. For longer times, the Hamiltonian in Eq. (57) is inadequate as it completely ignores the spatial evolution of the wave function. More sophisticated analysis motivated by this limitation is now available.[41]

4.4. *Nonlinear metrology using light-matter interfaces*

We briefly describe the only implementation of a nonlinear quantum metrology experiment that surpasses the Heisenberg limit. Consider $N \gg 1$ ultracold, trapped alkali atoms, with light pulses of macroscopic numbers of photons passing though them. The light is far from resonance to limit absorption but close enough that the optical nonlinearities are resonantly enhanced. Fast nonlinearities such as ac-Stark shifts and stimulated Raman transitions create atomic-spin-state-dependent interactions among the photons. The polarization state of the photons evolves in response to this interaction and is measured, allowing the spin polarization to be estimated. If the light field is given by $\mathbf{E} = \boldsymbol{\mathcal{E}} + \boldsymbol{\mathcal{E}}^*$, where $\boldsymbol{\mathcal{E}}$ is positive frequency part, the electric dipole interaction leads to an effective Hamiltonian

$$H_{\text{eff}} = \boldsymbol{\mathcal{E}}^* \cdot \overleftrightarrow{\alpha} \cdot \boldsymbol{\mathcal{E}}\,, \tag{68}$$

where $\overleftrightarrow{\alpha}$ is the polarizability tensor operator. Using the Stokes vector $\mathbf{S}$ to denote the optical degrees of freedom, the Hamiltonian can be decomposed into irreducible tensor components as[34]

$$H_{\text{eff}}^{(2)} = \alpha^{(1)} S_z J_z + \alpha^{(2)} (S_x J_x + S_y J_y)\,, \tag{69}$$

$$H_{\text{eff}}^{(4)} = \beta_J^{(0)} S_z^2 J_0 + \beta_N^{(0)} S_z^2 N_A + \beta^{(1)} S_0 S_z J_z + \beta^{(2)} S_0 (S_x J_x + S_y J_y)\,, \tag{70}$$

where the latter is obtained by using perturbation theory for the $F = 1$ manifold, N_A is the number of atoms, and related to the parameter to be estimated as $\langle J_z \rangle = N_A$. The terms proportional to $\alpha^{(1)}$ and $\beta^{(1)}$ describe the linear and nonlinear contributions to paramagnetic Faraday effect. For detunings Δ relative to the $F = 1 \to F' = 0$ in ^{87}Rb, both these parameters can be modulated to zero and nonzero

values. The precision in the estimate of F_z is given by

$$\delta F_z = \frac{1}{A(\Delta)N^{1/2} + B(\Delta)N^{3/2}}, \tag{71}$$

where N is the number of photons in the probe, a classical, gaussian light pulse, and $A(\Delta) \propto \alpha^{(1)}, B(\Delta) \propto \beta^{(1)}$.

The experiment[35] demonstrates a clear transition between the linear and nonlinear scaling of the precision. For an ideal nonlinear measurement, the improved scaling would guarantee better absolute sensitivity for sufficiently large values of N. Indeed, when the measurement bandwidth is taken into account, the nonlinear probe overtakes the linear one at $N = 3.2 \times 10^6$. Consequently, the nonlinear technique performs better in fast measurements. In contrast, when measurement time is not a limited resource, the comparison can be made on a "sensitivity-per-measurement" basis and the ideal crossover point, of 3.2×10^3 spins at $N = 8.7\times10^7$, is never actually reached, owing to the higher-order nonlinearities. Evidently, super-Heisenberg scaling allows but does not guarantee enhanced sensitivity: for the nonlinear technique to overtake the linear, it is also necessary that the scaling extend to large enough values of N. This experiment also shows that resource constraints dramatically influence the comparison between the linear and nonlinear techniques.

5. Conclusion

The aim of this review was to investigate the qualitative and the quantitative roles of entanglement in quantum enhanced metrology. Or in other words, is entanglement necessary to provide quantum enhancements in metrology, and if so how much enhancement can it provide? We have shown it is possible to surpass the erstwhile Heisenberg limit of $1/N$ for the precision of estimating parameters allied to a nonlinear Hamiltonian without preparing entangled states, and that when entanglement is present, it can provide at most a square root improvement in the scaling of the measurement precision. The connection to Grover's search algorithm is suggestive, which attains improvements of $\mathcal{O}(\sqrt{N})$ in search problems without the use of entanglement but only superpositions.[17]

The resources that go into the quantum limited measurement are quantified in our discussion in terms of the number of particles or the time invested, it could also be other resources such as energy or space-time volume. Time or energy are natural resources, while space could correspond to number of modes involved. Resources accounting is additionally important in lossy quantum metrology where techniques such as post-selection provide a skewed reckoning of the resources invested. Nevertheless, quantum enhancements are possible in lossy implementations of quantum metrology.[49–55] Recently, efforts have also been made to use a quantum query complexity type argument to count the number of basic gates that make up the interaction Hamiltonian.[56,57] However, they suffer from the intrinsic drawback that naturally occurring parameter estimation strategies do not necessarily operate in that manner. It is a property of the particular quantum state the system is in

that decides the precision of the estimate. For instance, the ground state solutions of BECs provide precision scalings $\sim 1/N^{3/2}$, while solitonic solutions[58] of the same system provides scaling $\sim 1/N^{3/4}$ in estimating displacements.

All quantum enhancements in metrology can be traced back to two basic effects. One is the accelerated accumulation of relative phase in a superposition state of the eigenvectors corresponding to the maximum and minimum eigenvalues of the generator Hamiltonian, for instance in Eq. (4). The other is the suppression of noise and improvement of the signal-to-noise ratio by effects such as squeezing. The latter is definitely nonclassical, and can be thought of as a precursor of quantum entanglement.[59] The former can, as we have shown, exist independently of entanglement. As is well known, entanglement is not sufficient for quantum enhancements in metrology.[60] It has also been suggested that other forms of quantum correlations, such as quantum discord, might provide quantum advantages.[61] Eventually, the scaling of resources invested with palpable quantum advantages is the ultimate benchmark for quantum enhanced metrology, and the identification of necessary resources a central task of the field.

Acknowledgments

It is a pleasure to thank C. M. Caves, S. Boixo, S. T. Flammia, A. Tacla, L. Zhang, X. M. Jin, I. A. Walmsley for several interesting and stimulating discussions. This work was funded in part by EPSRC (Grant EP/H03031X/1), US EOARD (Grant 093020), and EU Integrated Project Q-ESSENCE. AS acknowledges the support of the Department of Science and Technology, Government of India, through the fast-track scheme for young scientist, grant No. 100/IFD/5771/2010-11.

References

1. L. Mandelstam and I. Tamm, *Izv. Akad. Nauk. SSSR Ser. Fiz.* **9** (1945) 122 [*J. Phys.* (*Moscow*) **9** (1945) 249].
2. K. S. Thorne, R. W. P. Drever, C. M. Caves, M. Zimmermann and V. D. Sandberg, *Phys. Rev. Lett.* **40** (1978) 667.
3. C. M. Caves, K. S. Thorne, R. W. P. Drever, V. D. Sandberg and M. Zimmermann, *Rev. Mod. Phys.* **52** (1980) 341.
4. V. B. Braginsky, Y. I. Vorontsov and K. S. Thorne, *Science* **209** (1980) 547.
5. C. M. Caves, *Phys. Rev. D* **23** (1981) 1693.
6. J. Abadie *et al.*, *Nat. Phys.* **7** (2011) 962.
7. S. M. Barnett, C. Fabre and A. Maitre, *Eur. Phys. J. D* **22** (2003) 513.
8. R. S. Bondurant and J. H. Shapiro, *Phys. Rev. D* **30** (1984) 2548.
9. M. J. Holland and K. Burnett, *Phys. Rev. Lett.* **71** (1993) 1355.
10. B. C. Sanders and G. J. Milburn, *Phys. Rev. Lett.* **75** (1995) 2944–2947.
11. J. J. Bollinger, W. M. Itano, D. J. Wineland and D. J. Heinzen, *Phys. Rev. A* **54** (1996) R4649.
12. B. C. Sanders, *Phys. Rev. A* **40** (1989) 2417.
13. V. Giovannetti, S. Lloyd and L. Maccone, *Nat. Photon.* **5** (2011) 222.
14. V. Giovannetti, S. Lloyd and L. Maccone, *Science* **306** (2004) 1330.

15. L. Maccone and G. De Cillis, *Phys. Rev. A* **79** (2009) 023812.
16. S. D. Bartlett, T. Rudolph and R. W. Spekkens, *Rev. Mod. Phys.* **79** (2007) 555.
17. D. A. Meyer, *Phys. Rev. Lett.* **85** (2000) 2014.
18. S. Lloyd, *Science* **321** (2008) 1463.
19. J. H. Shapiro and S. Lloyd, *New J. Phys.* **11** (2009) 063045.
20. S.-H. Tan, B. I. Erkmen, V. Giovannetti, S. Guha, S. Lloyd, L. Maccone, S. Pirandola and J. H. Shapiro, *Phys. Rev. Lett.* **101** (2008) 253601.
21. B. L. Higgins, D. W. Berry, S. D. Bartlett, H. M. Wiseman and G. J. Pryde, *Nature* **49** (2007) 393.
22. S. Boixo, C. M. Caves, A. Datta and A. Shaji, *Laser Phys.* **16** (2006) 1525.
23. A. Luis, *Phys. Lett. A* **329** (2004) 8.
24. J. Beltrán and A. Luis, *Phys. Rev. A* **72** (2005) 045801.
25. S. Boixo, S. T. Flammia, C. M. Caves and J. M. Geremia, *Phys. Rev. Lett.* **98** (2007) 090401.
26. A. M. Rey, L. Jiang and M. D. Lukin, *Phys. Rev. A* **76** (2007) 053617.
27. S. Boixo, A. Datta, S. T. Flammia, A. Shaji, E. Bagan and C. M. Caves, *Phys. Rev. A* **77** (2008) 012317.
28. S. Boixo, A. Datta, M. J. Davis, S. T. Flammia, A. Shaji and C. M. Caves, *Phys. Rev. Lett.* **101** (2008) 040403.
29. S. Choi and B. Sundaram, *Phys. Rev. A* **77** (2008) 053613.
30. M. J. Woolley, G. J. Milburn and C. M. Caves, *New J. Phys.* **10** (2008) 125018.
31. S. Boixo, A. Datta, M. J. Davis, A. Shaji, A. B. Tacla and C. M. Caves, *Phys. Rev. A* **80** (2009) 032103.
32. A. B. Tacla, S. Boixo, A. Datta, A. Shaji and C. M. Caves, *Phys. Rev. A* **82** (2010) 053636.
33. Á. Rivas and A. Luis, *Phys. Rev. Lett.* **105** (2010) 010403.
34. M. Napolitano and M. W. Mitchell, *New J. Phys.* **12** (2010) 093016.
35. M. Napolitano, M. Koschorreck, B. Dubost, N. Behbood, R. J. Sewell and M. W. Mitchell, *Nature* **471** (2011) 486.
36. S. L. Braunstein and C. M. Caves, *Phys. Rev. Lett.* **72** (1994) 3439.
37. S. L. Braunstein, C. M. Caves and G. J. Milburn, *Ann. Phys.* **247** (1996) 135.
38. C. W. Helstrom, *Quantum Detection and Estimation Theory* (Academic Press, New York, 1976).
39. A. S. Holevo, *Probabilistic and Statistical Aspects of Quantum Theory* (North-Holland, Amsterdam, 1982).
40. M. F. Riedel, P. Böhi, Y. Li, T. W. Hänsch, A. Sinatra and P. Treutlein, *Nature* **464** (2010) 1170.
41. A. B. Tacla and C. M. Caves, *Phys. Rev. A* **84** (2011) 053606.
42. S. M. Roy and S. L. Braunstein, *Phys. Rev. Lett.* **100** (2008) 220501.
43. A. J. Leggett, *Rev. Mod. Phys.* **73** (2001) 307.
44. C. W. Pethick and H. Smith, *Bose Einstein Condensation in Dilute Gases* (Cambridge University Press, Cambridge, 2002).
45. F. Dalfovo, S. Giorgini, L. P. Pitaevskii and S. Stringari, *Rev. Mod. Phys.* **71** (1999) 463.
46. C.-H. Lee, J.-H. Huang, H.-M. Deng, H. Dai and J. Xu, arXiv:1110.4734 (2011).
47. K. M. Mertes, J. W. Merrill, R. Carretero-González, D. J. Frantzeskakis, P. G. Kevrekidis and D. S. Hall, *Phys. Rev. Lett.* **99** (2007) 190402.
48. G.-B. Jo, J.-H. Choi, C. A. Christensen, Y.-R. Lee, T. A. Pasquini, W. Ketterle and D. E. Pritchard, *Phys. Rev. Lett.* **99** (2007) 240406.
49. A. Shaji and C. M. Caves, *Phys. Rev. A* **76** (2007) 032111.

50. U. Dorner, R. Demkowicz-Dobrzanski, B. J. Smith, J. S. Lundeen, W. Wasilewski, K. Banaszek and I. A. Walmsley, *Phys. Rev. Lett.* **102** (2009) 040403.
51. R. Demkowicz-Dobrzanski, U. Dorner, B. J. Smith, J. S. Lundeen, W. Wasilewski, K. Banaszek and I. A. Walmsley, *Phys. Rev. A* **80** (2009) 013825.
52. M. Kacprowicz, R. Demkowicz-Dobrzanski, W. Wasilewski, K. Banaszek and I. A. Walmsley, *Nat. Photon.* **4**(6) (2010) 357.
53. N. Thomas-Peter, B. J. Smith, A. Datta, L.-J. Zhang, U. Dorner and I. A. Walmsley, *Phys. Rev. Lett.* **107** (2011) 113603.
54. A. Datta, L.-J. Zhang, N. Thomas-Peter, U. Dorner, B. J. Smith and I. A. Walmsley, *Phys. Rev. A* **83** (2011) 063836.
55. B. M. Escher, R. L. de Matos Filho and L. Davidovich, *Nat. Phys.* **7** (2011) 406.
56. M. Zwierz, C. A. Pérez-Delgado and P. Kok, *Phys. Rev. Lett.* **105** (2010) 180402.
57. M. Zwierz, C. A. Pérez-Delgado and P. Kok, arXiv:1201.2225 (2012).
58. A. Negretti, C. Henkel and K. Mølmer, *Phys. Rev. A* **78** (2008) 023630.
59. J. K. Asbóth, J. Calsamiglia and H. Ritsch, *Phys. Rev. Lett.* **94** (2005) 173602.
60. P. Hyllus, O. Gühne and A. Smerzi, *Phys. Rev. A* **82** (2010) 012337.
61. K. Modi, H. Cable, M. Williamson and V. Vedral, *Phys. Rev. X* **1** (2011) 021022.